ISSN 1990-7931, Russian Journal of Physical Chemistry B, 2019, Vol. 13, No. 2, pp. 328–338. © Pleiades Publishing, Ltd., 2019.
Russian Text © The Author(s), 2019, published in Khimicheskaya Fizika, 2019, Vol. 38, No. 3, pp. 52–63.

CHEMICAL PHYSICS OF ECOLOGICAL PROCESSES

Analysis of Breakthrough Curves of Dynamic Adsorptive Removal of Pollutants from Water

I. V. Kumpanenko[a], *, N. A. Ivanova[a], M. V. Dyubanov[a], O. V. Shapovalova[a], A. A. Solov'yanov[a], and A. V. Roshchin[a]

[a] *Semenov Institute of Chemical Physics, Russian Academy of Sciences, Moscow, 119991 Russia*

**e-mail: ivkumpan@chph.ras.ru*

Received June 29, 2018; revised September 5, 2018; accepted September 20, 2018

Abstract—A comparative analysis is made of mathematical models of breakthrough curves $C/C_0 = f(t)$ describing the removal of pollutants from water, where C_0 and C are the pollutant concentrations in water flows at the inlet and outlet of an adsorption column, respectively, and t is current time. It is shown that, within the Thomas and BDST (bed depth service time) models, the time dependence of breakthrough concentration C is described by the linear equation $\ln(C_0/C - 1) = a_0 - a_1 t$, where a_0 and a_1 are coefficients, which have different meanings in different models. Approximation of experimental dependences by this linear theoretical dependence enables locating these coefficients and then, using them, calculating adsorption parameters, in particular, the adsorption rate constant k and dynamic adsorption capacity q_m. These parameters are determined for processes described in the literature, namely, dynamic adsorption of Hg(II) on granulated activated carbon and activated carbon cloth and dynamic adsorption of nitrate ions on commercial anion-exchange resin PA408.

Keywords: dynamic adsorption, fixed adsorbent bed, breakthrough curve, adsorption rate constant, dynamic adsorption capacity, mathematical models of adsorption

DOI: 10.1134/S1990793119020040

1. INTRODUCTION

Dynamic adsorption is widely used for treatment of industrial waste gases, and drinking and waste water [1]. Dynamic adsorption typically occurs in open systems, where a gas or liquid flow containing pollutants passes through a column packed with an adsorbent, which removes the pollutants from the flow. The most important characteristics of dynamic column adsorption are found through the analysis of breakthrough (elution) curves, which describe the dependences of the concentrations of substances in the mobile phase at the column outlet on time or elution solvent volume. Breakthrough curves are generally curves of ratio $C(t)/C_0$ versus time, where $C(t)$ is the analyte concentration at the sorption column outlet at time t, and C_0 is the initial analyte concentration at the column inlet.

A breakthrough curve can be analyzed using an adequate mathematical model. In one of our previous articles [1], based on a preliminarily analysis of the shapes of the experimental breakthrough curves we obtained, we showed that dynamic adsorption of the simplest inorganic substances, such as nitrogen oxides, from an air flow on zeolites is best described by the Wheeler–Jonas model [2–5].

In this work, we studied dynamic adsorption of some pollutants dissolved in water by a fixed bed of adsorbent. The study was conducted by comparing various mathematical models [6–10] used for describing experimental breakthrough curves taken from the literature.

2. MATHEMATICAL MODELS OF DYNAMIC COLUMN ADSORPTION

A model describing the dynamic adsorption of a pollutant in a fixed adsorbent bed from the liquid phase was chosen based on the quality of approximation of experimental breakthrough curves by theoretical ones using this model. Unlike adsorption in the gas–solid system, theoretical description of dynamic adsorption in the liquid–solid system is complicated by the more complex pattern of interactions in the liquid solution between particles participating in the process, which is considerably affected by solvation.

Broadly, the mechanism of dynamic column adsorption of a pollutant from the liquid phase in a fixed adsorbent bed includes four steps (Fig. 1):

— mass transfer of pollutant molecules in the liquid phase, which includes convection (region *1*) and molecular diffusion (*2*);

— diffusion at the liquid–adsorbent surface interface (*3*);

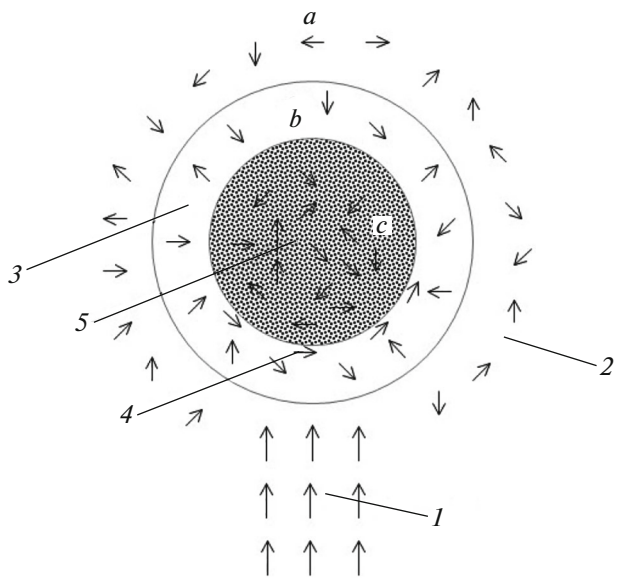

Fig. 1. Scheme of four-step adsorption of a pollutant from the liquid phase on an adsorbent granule: (*a*) liquid phase, (*b*) liquid–adsorbent surface interface (film), and (*c*) adsorbent granule; (*1*) convection, (*2*) molecular diffusion, (*3*) diffusion at the liquid–adsorbent surface interface, (*4*) surface diffusion, and (*5*) diffusion in adsorbent pores.

— mass transfer within the granule, including surface diffusion (*4*) and diffusion in adsorbent pores (*5*);

— adsorption–desorption reactions on the surface of granules and pores.

A decisive role in choosing a dynamic adsorption model is played by the material balance equation (macroscopic mass conservation law), adsorption rate equation, and adsorption isotherm. Features of the adsorption system, such as adsorbate, adsorbent, solvent, and process conditions, should also be taken into account. Another important aspect is also the generality of a chosen model because the model applicability in many cases is limited by ranges of time, concentration, adsorbent bed depth, and other aspects.

A significant part is played by the mechanism of diffusion on the surface of adsorbent granules and in pores. Under the assumption that the intragranular diffusion obeys Fick's laws, several models for describing the mass-transfer rate were proposed: a pore diffusion model [11], a homogeneous surface diffusion model [12], and a parallel pore/surface diffusion model [13]. Here, one can also refer to a linear driving force model [14], in which the equation of the intragranular diffusion rate is linear, and to a wave theory model [15].

Theoretical breakthrough curves in the above models are generally calculated numerically by solving partial differential equations for initial and boundary conditions, which complicates the analysis of experimental breakthrough curves. At the same time, in several models (presented below), breakthrough curves are described by simple analytical expressions.

Bohart–Adams Model [16–18]

This model was first obtained by studying pollutant adsorption in an air flow. Bohart and Adams presented this model in the course of the investigation of chlorine adsorption by charcoal [16]. They assumed that the chlorine adsorption rate in a sorption column would be proportional to the chlorine concentration in the air and to the residual adsorption capacity of the charcoal. Under these assumptions, one can show that the pollutant adsorption from the air flow on the surface of the adsorbent is described by the system of equations [19]:

$$\frac{\partial C}{\partial z} = -\frac{k_{BA} q \rho C}{u}, \qquad \frac{\partial q}{\partial t} = -k_{BA} q C, \tag{1}$$

where C (mg/mL) is the pollutant concentration in the air flow, z (cm) is the distance from the inlet of the sorption bed to a point under consideration along the bed axis, t (min) is current time, q (mg/g) is the residual sorption capacity of the adsorbent at time t, ρ (g/cm^3) is the apparent density of the adsorbent, u (cm/min) is the linear flow velocity, and k_{BA} (mL mg^{-1} min^{-1}) is the Bohart–Adams adsorption rate constant.

Under initial and boundary conditions, $q = q_m$ at $t = 0$ and $C = C_0$ at $z = 0$ (q_m (mg/g) is the dynamic adsorption capacity (DAC) of the adsorbent (the maximum possible pollutant concentration in the adsorbent), and C_0 (mg/mL) is the initial pollutant concentration in the air), solving the system of Eqs. (1) gives the following dependence of C/C_0 on time t for dynamic pollutant adsorption according to the Bohart–Adams model:

$$\ln\left(\frac{C_0}{C} - 1\right) = \ln\left[\exp\left(k_{BA} q_m \frac{H\rho}{u}\right) - 1\right] - k_{BA} C_0 t; \tag{2}$$

where H (cm) is the depth of the adsorbent bed in the column.

Note that the Bohart–Adams equation adequately describes the dependence of C/C_0 on t in the initial portion of the breakthrough curve, i.e., for small t [17].

BDST Model [20]

If $\exp\left(k_{BA} q_m \frac{H\rho}{u}\right) \gg 1$, then Eq. (2) takes much simpler form

$$t = \frac{q_m H \rho}{C_0 u} - \frac{1}{k_{BA} C_0} \ln\left(\frac{C_0}{C} - 1\right). \tag{3}$$

This model, which is typically referred to as the bed depth service time (BDST) model [17, 18], is charac-

terized by a linear dependence between the depth H of the adsorbent bed in a column and the time t until pollutant breakthrough. The breakthrough concentration versus time curve (breakthrough curve) in the BDST model is often described by the expression

$$\ln\left(\frac{C_0}{C}-1\right)=\frac{k_{BA}q_m H\rho}{u}-k_{BA}C_0 t. \quad (4)$$

As noted above, this model is based on the assumption that the sorption rate is controlled by the surface reaction between the adsorbate and the unreacted adsorbent.

Yoon–Nelson Model [8, 21–23]

Yoon and Nelson [21] developed this relatively simple model for describing dynamic adsorption and adsorbate breakthrough in the sorption bed of activated coal. In this model, the following formula is valid:

$$\ln\left(\frac{C_0}{C}-1\right)=k_{YN}t_{1/2}-k_{YN}t, \quad (5)$$

where k_{YN} (min^{-1}) is the Yoon–Nelson adsorption rate constant, and $t_{1/2}$ (min) is the time in which the adsorbate concentration in the flow reaches $0.5C_0$.

The Yoon–Nelson model is one of the simplest of the existing models, and using it requires no additional data on characteristics of adsorbate, type of adsorbent, and physical properties of sorption bed. Although Bohart–Adams equation (2) and Yoon–Nelson equation (5) were originally derived to describe adsorption of a substance from an air flow [16, 21], it has been further shown that they adequately represent dynamic adsorption from an aqueous medium [8, 17, 18, 22].

Thomas Model

The Thomas model is based on the assumption that a reversible adsorption reaction is described by a second-order kinetic equation and that the dependence of the amount of the adsorbed pollutant on the pollutant concentration in the mobile phase obeys the Langmuir isotherm equation [9, 10]. Theoretically, this model is suitable for describing an adsorption process in which the internal and external diffusion resistances are extremely low [8]. The Thomas model is most often used for characterizing the behavior of breakthrough curves of dynamic adsorption of substances from aqueous solutions in a fixed adsorbent bed. According to this model, the dependence of the pollutant concentration C (mg/mL) at the outlet of an adsorption column on time t (min) is described by the equation

$$\ln\left(\frac{C_0}{C}-1\right)=k_{Th}\frac{q_m M}{Q}-k_{Th}C_0 t, \quad (6)$$

where k_{Th}(mL mg^{-1} min^{-1}) is the Thomas adsorption rate constant, M (g) is the weight of the adsorbent in the column, and Q (mL/min) is the volumetric flow rate of the solution flow being treated.

Because

$$\frac{H\rho}{u}=\frac{HS\rho}{uS}=\frac{M}{Q}, \quad (7)$$

where S (cm^2) is the cross-sectional area of the adsorbent bed in the column, Eqs. (4) and (6) formally differ only by the adsorption rate constants k_{BA} and k_{Th}. Consequently, although the assumptions and procedures used in deriving the BDST and Thomas models differ, the equations of the time dependence of breakthrough pollutant concentration in these models are the same. It should be noted that the Bohart–Adams model and the BDST model, which is derived from it, describe the dependence of C/C_0 on t well only in the initial portion of the breakthrough curve [17], whereas the Thomas model is valid throughout the t range.

A distinguishing feature of the BDST, Yoon–Nelson, and Thomas models is a linear dependence of $\ln(C_0/C-1)$ on time t (compare Eqs. (4), (5), and (6)). Note at once that, within the same models, a linear time dependence is also observed for the function $\ln\{C/(C_0-C)\}$, which is equal to $-\ln(C_0/C-1)$.

One can see from Eq. (4) or (6) that, by constructing experimental $\ln(C_0/C-1)$ versus t curves, one can determine the quantities $k_{BA}q_m H\rho/u$ or $k_{Th}q_m M/Q$ (y-intercepts), and the quantities $k_{BA}C_0$ or $k_{Th}C_0$ (slopes).

The Yoon–Nelson model differs significantly from the other two models in that that the slope of the linear function of $\ln(C_0/C-1)$ versus t in Eq. (5) is exactly equal to the Yoon–Nelson adsorption rate constant k_{YN} and is independent of any other process parameters, whereas the respective slopes in the BDST and Thomas models are also dependent on (proportional to) the initial pollutant concentration C_0 in the solution. This fact makes it possible to determine which of the models can describe the dynamic adsorption process under consideration.

Equations (4)–(6) can be represented in the general form

$$\ln\left(\frac{C_0}{C}-1\right)=a_0-a_1 t, \quad (8)$$

where the parameters a_0 and a_1 are different in different equations (Table 1).

Note that all the parameters presented in Table 1 are positive: k_{BA}, q_m, H, ρ, u, k_{YN}, $t_{1/2}$, M, k_{Th}, Q, $C_0 > 0$; therefore, a_0 and $a_1 > 0$.

Table 1. Parameters a_0 and a_1 in Eq. (8) for various models

Equation/model	a_0	a_1
(4)/BDST	$\frac{k_{BA}q_m H\rho}{u}$	$k_{BA}C_0$
(5)/ Yoon–Nelson	$k_{YN}t_{1/2}$	k_{YN}
(6)/Thomas	$k_{Th}\frac{q_m M}{Q}$	$k_{Th}C_0$

$k_{BA} = k_{Th} = k$.

Transformation of Eq. (8) gives the expression for breakthrough curve:

$$y = \frac{C}{C_0} = \frac{1}{1 + \exp(a_0 - a_1 t)}. \quad (9)$$

Formula (9) at a_0, $a_1 > 0$ describes an increasing logistic curve [6, 24, 25] (Fig. 2). Such curves have then following properties:

– asymptote $y = 1$ as $t \to +\infty$,

– asymptote $y = 0$ as $t \to -\infty$,

– point of inflection ($t = a_0/a_1$, $y = 0.5$),

– downward concavity at $t < a_0/a_1$ and upward concavity at $t > a_0/a_1$,

– slope $y = y(t)$ approaches zero only as $t \to \pm\infty$,

– function $y = y(t)$ is continuous throughout the range $-\infty < t < +\infty$.

Besides, logistic curves described by an equation of the type of Eq. (9) are characterized by symmetry, the element of which is the center of inversion i (Fig. 2) at the point of inflection ($t = a_0/a_1$, $y = 0.5$). Here, by symmetry, we mean not the symmetry of an individual curve, but the symmetry of a curve in a coordinate system.

To show that inversion transforms a logistic curve into exactly the same curve, let us consider the transformation of Eq. (9) by inversion of coordinates. The inversion of coordinates $t \to t'$ and $y \to y'$ about the point i can be represented as $y = 1 - y'$ and $t = 2a_0/a_1 - t'$. After this transformation of coordinates, Eq. (9) takes the form

$$1 - y' = \left[1 + \exp\left\{a_0 - a_1\left(\frac{2a_0}{a_1} - t'\right)\right\}\right]^{-1}. \quad (10)$$

Further transformations can transform Eq. (10) to a form identical to Eq. (9):

$$y' = \frac{1}{1 + \exp(a_0 - a_1 t')}. \quad (11)$$

This result confirms the inversion symmetry of the logistic curve in Fig. 2. Similar results can also be obtained by rotation of the curve by an angle of 180° about the axis C_2, which passes through the point i and is perpendicular to the plane (y, t), or by two sequential reflections in the planes σ_v, which pass through the point i and are perpendicular to the plane (y, t) (the intersections of the planes σ_v with the plane (y, t) are shown in Fig. 2 by dashed lines).

Note that this symmetry is characteristic of breakthrough curves of dynamic adsorption described by the BDST, Yoon–Nelson, and Thomas models, which are characterized by a linear dependence of $\ln(C_0/C - 1)$ on t, represented in the general form by Eq. (8). However, the corresponding experimental dependences often deviate from linearity.

Some researchers [6, 19] have noticed a mathematical similarity between logistic-type curves of breakthrough concentrations versus time under dynamic adsorption of substances on adsorbents with finite adsorption capacity and population growth in various countries [26, 27]. By analogy with the theoretical analysis of population growth, in the case of deviation of the experimental curve $\ln(C_0/C - 1) = f(t)$ from linearity, it has been proposed to use its generalized version in the form of a power series [28]:

$$\ln\left(\frac{C_0}{C} - 1\right) = \sum_{i=0}^{N} b_i t^i. \quad (12)$$

The comparison of expressions (8) and (12) gives that $b_0 = a_0$ and $b_1 = -a_1$.

The expression for the breakthrough curve in this case takes the form

$$\frac{C}{C_0} = \frac{1}{1 + \exp\left(\sum_{i=0}^{N} b_i t^i\right)}. \quad (13)$$

In the next section of this article, some experimental dependences of $\ln(C_0/C - 1)$ on t, which were taken from the literature, are approximated using Eq. (8) or (12). For simplicity, we will not distinguish between the BDST and Thomas models and will refer to them collectively as the

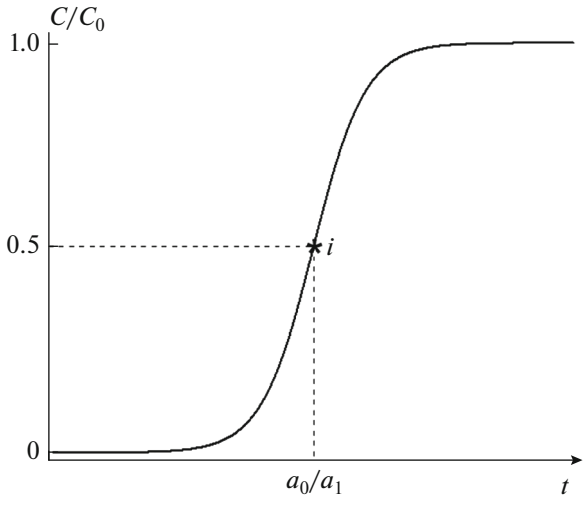

Fig. 2. Logistic curve described by Eq. (9).

BDST model. The adsorption rate constant for these models will be denoted by k (mL mg^{-1} min^{-1}).

3. THEORETICAL ANALYSIS OF EXPERIMENTAL TIME DEPENDENCES OF BREAKTHROUGH ADSORBATE CONCENTRATION

Experimental breakthrough curves for various adsorbate–adsorbent systems can more or less strongly deviate from the ideal shape of the symmetric logistic curve shown in Fig. 2. This fact is unambiguously related to the possibility (or impossibility) of describing an experimental time dependence of $\ln(C_0/C - 1)$ by a straight line: the more ideal logistic curve, the higher the probability of linearization of this dependence. Let us consider several examples of the description of experimental dependences taken from scientific literature in linear (see Eq. (8)) and/or nonlinear (see Eq. (12)) coordinates and subsequent calculations of parameters of adsorption processes.

Dynamic Adsorption of Hg(II) Ions on a Fixed Bed of Activated Carbon

Goyal et al. [29] studied the adsorption of Hg(II) ions on activated carbon cloth (HEG, Bhopal, India) and I-50 granulated activated carbon (Carbons Private Limited, Ankleshwar, India) in a dynamic mode in a continuous column reactor in water treatment. Table 2 presents the conditions of Goyal et al. experiments after conversion to units of measure used in this work. The sets of constant parameter values are the same in all the experiments on various adsorbents.

The primary data for all of Goyal et al. experiments [29] were represented as breakthrough curves, i.e., dependences of C/C_0 on t. The experimental results were mathematically processed within the BDST model using Eq. (3). In particular, Goyal et al. [29] constructed dependences of t on H and approximated them by straight lines. In this work, the primary data taken from Goyal et al. article [29] were also processed within the BDST model, however, using Eq. (4) or generalized formula (8). Specifically, dependences of $\ln(C_0/C - 1)$ on t were constructed, and by approximating them by straight lines, the parameters given in Table 1 were determined.

In our opinion, this approach shows a more illustrative insight into the adsorption process and facilitates mathematical processing. With account of Eq. (7), the conclusions drawn by such a consideration are also consistent with the Thomas model.

Unfortunately, Goyal et al. [29] did not indicate the apparent densities ρ of the used adsorbents, which are necessary for mathematical processing of the experimental data. However, we succeeded in filling this gap through the method described below.

Table 2. Experimental conditions

H, cm	u, cm/min	C_0, mg/mL
8	10.167	0.05
10	7.167	0.10
15	5	0.15

Figure 3 shows the breakthrough curves, which were constructed using Goyal et al. data [29] and describe the mercury adsorption on adsorbents of two types: activated carbon cloth (ACC) and granulated activated carbon (GAC). The experimental conditions are given in the figure caption.

We constructed $\ln(C_0/C - 1)$ versus t curves according to Eq. (8) using the C/C_0 values taken from Fig. 3. Figure 4 shows the obtained curves in linearizing coordinates. Table 3 presents the parameters a_0 and a_1 of the straight lines shown in Fig. 4, which were determined during approximation of experimental dependences by Eq. (8).

As follows from Table 1, the adsorption rate constants were calculated by the formula

$$k = k_{BA} = a_1/C_0, \tag{14}$$

and the density of adsorbents was found by the expression

$$\rho = \frac{a_0 u}{k q_m H}. \tag{15}$$

The adsorbent DAC q_m, which depends on the velocity u of the liquid in the column, was determined experimentally by Goyal et al. [29].

Note that the ACC density value ρ = 0.184 g/cm^3 we determined is within the range of ordinary values of

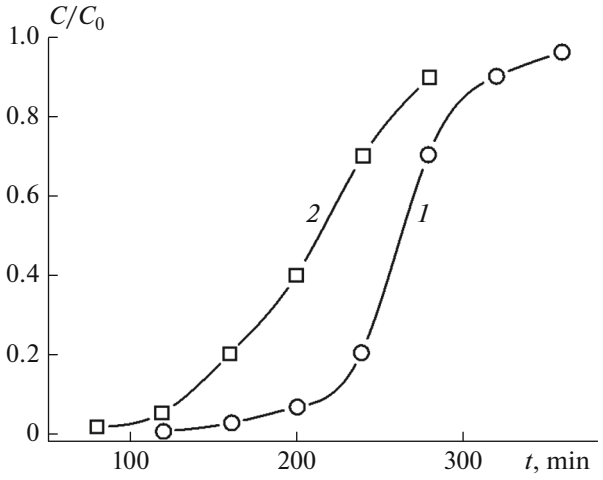

Fig. 3. Breakthrough curves of dynamic adsorption of Hg(II) on the adsorbents (*1*) ACC and (*2*) GAC at H = 10 cm, C_0 = 0.05 mg/mL, and u = 7.167 cm/min [29].

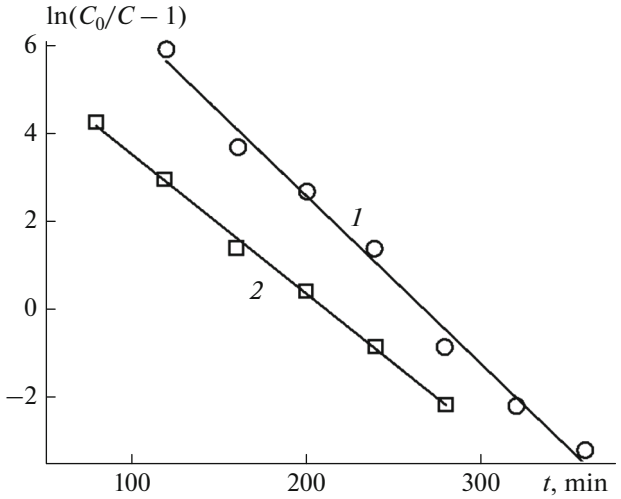

Fig. 4. $\ln(C_0/C - 1)$ versus t curves of dynamic adsorption of Hg(II) on the adsorbents (*1*) ACC and (*2*) GAC that were constructed based on Goyal et al. data [29] shown in Fig. 3.

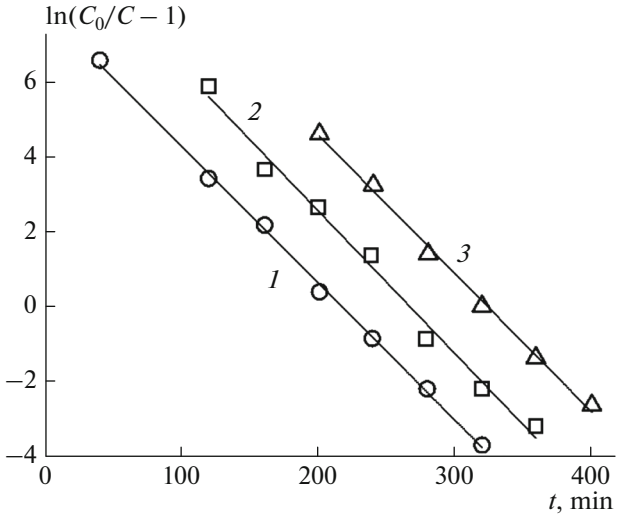

Fig. 5. $\ln(C_0/C - 1)$ versus t curves of dynamic adsorption of Hg(II) on the adsorbent ACC at $H = 10$ cm; $C_0 = 0.05$ mg/mL; and various velocities of the solutions being treated of $u =$ (*1*) 10.167, (*2*) 7.167, and (*3*) 5.0 cm/min.

apparent densities of activated carbon cloths. For example, the apparent densities of activated carbon cloths produced by the Purair Carbon Filter Company (China) are within the range 0.06–0.3 g/cm^3. The calculated GAC density $\rho = 0.568$ g/cm^3 is close to the apparent density 0.551 g/cm^3 of KG-CAB granulated activated carbon produced by UES (Ueda Environmental Solutions) Co., Ltd. The density values we determined are used below for processing the data of subsequent experiments. The caption of Fig. 3 presents some of the experimental conditions. Table 3 also gives the coefficients of determination R^2, the values of which (~0.99) are indicative of high quality of approximation of the experimental data by straight lines.

Effect of the Solution Velocity in the Fixed Adsorbent Bed on the Mercury Adsorption Process

Using the proposed approach, we processed Goyal et al. experimental data [29] on the breakthrough curves of dynamic adsorption of mercury on ACC and GAC at three velocities of the solutions being treated and three depths of the fixed adsorbent bed (Table 2).

Figures 5 and 6 present the $\ln(C_0/C - 1)$ versus t curves we constructed for ACC and GAC, respectively. The captions of these figures give the experimental conditions. As Figs. 5 and 6 show, the experimental points lie on straight lines with small scatter in all the dynamic adsorption experiments at various solution velocities in the fixed adsorbent bed.

Table 3. Parameters a_0 and a_1 determined by approximation and the given and calculated experimental parameters of dynamic adsorption of Hg(II) on the adsorbents ACC and GAC

Adsorbent	a_0	a_1	R^2	k	q_m	ρ
ACC	10.196	0.0381	0.989	0.763	52.077	0.184
GAC	6.682	0.0316	0.997	0.633	13.31	0.568

The straight lines were obtained by approximating the experimental dependences by Eq. (8). Determined during the approximation, the parameters a_0 and a_1 of the straight lines are given in Table 4. This table also presents the coefficients of determination R^2, which suggest high quality of approximation of the experimental dependences by straight lines ($R^2 \sim 0.99$), as well as the adsorption rate constants k and the adsorbent DAC q_m at various treatment velocities as calculated by the formulas of Table 1. In the calculations, the adsorbent densities ρ determined in preliminary experiments and given in Table 3 were used.

The values (~0.99) of the coefficients of determination indicate high goodness of fit and linearity of the dependence of $\ln(C_0/C - 1)$ on t at small scatter of experimental data about the approximating straight lines. Figures 5 and 6 show that the slopes of the curves of adsorption on both ACC and GAC are close. This fact is also indicated by the similarity of the parameters a_1 of these adsorbents (Table 4).

In the BDST model, $a_1 = kC_0$ (Table 1), and the experiments were carried out at the same initial solution concentration C_0 (0.05 mg/mL); therefore, the adsorption rate constants k for each of the adsorbents are similar and are within the ranges 0.732–0.763 and 0.592–0.633 mL mg^{-1} min^{-1} for ACC and GAC, respectively. The mean linear deviations $\sum_{i=1}^{N} |k_i - \bar{k}| / N$ of the constants k do not exceed 2.4 and 4.1% for ACC and GAC, respectively.

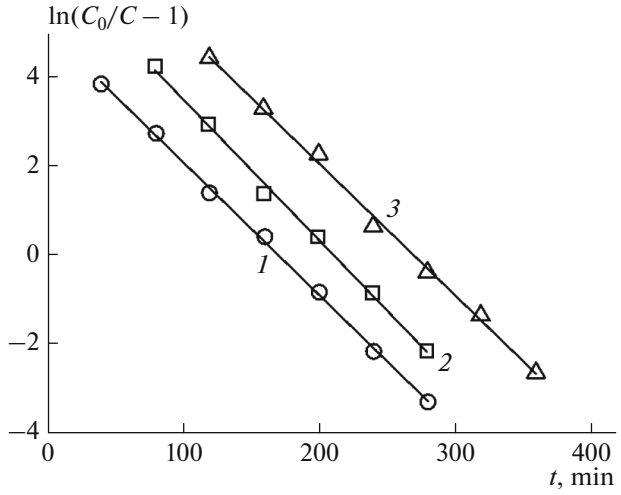

Fig. 6. $\ln(C_0/C-1)$ versus t curves of dynamic adsorption of Hg(II) on the adsorbent GAC at H = 10 cm; C_0 = 0.05 mg/mL; and various velocities of the solutions being treated of u = (*1*) 10.167, (*2*) 7.167, and (*3*) 5.0 cm/min.

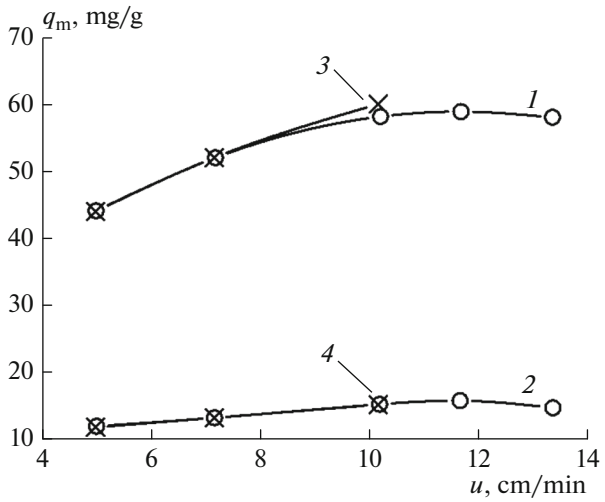

Fig. 7. DAC of (*1*, *3*) ACC and (*2*, *4*) GAC versus linear velocity of the liquid flow: (*1*, *2*) (–○–) experimental data [29], (*3*, *4*) (–×–) calculated q_m values (Table 4), H = 10 cm, and C_0 = 0.05 mg/mL.

Using the values of the parameters u, a_0, k, and H (Table 4) and ρ (Table 3), we calculated the adsorbent DAC q_m, which depends on the solution velocity, by the formula (Table 1):

$$q_m = \frac{a_0 u}{kH\rho}. \quad (16)$$

The calculated q_m values are presented in Table 4 and shown in Fig. 7 in comparison with the q_m values determined experimentally by Goyal et al. [29]. As is seen from Fig. 7, the calculated values of q_m agree with its experimental data with high accuracy. A small discrepancy is observed only for ACC (curve *3*) at a liquid velocity of u = 10.167 cm/min.

We remind that, in our calculations, we used the values of the apparent densities ρ of the adsorbents that we calculated during processing Goyal et al. experimental data [29] on adsorption on ACC and GAC at only one liquid velocity (7.167 cm/min). The agreement of the calculated and experimental data at the other velocities is indicative of the adequacy of our proposed approach to mathematical processing of experimental results.

Effect of the Depth of the Fixed Adsorbent Bed on the Mercury Adsorption Process

Similar to what we did in the previous subsection, in this subsection, we constructed $\ln(C_0/C-1)$ versus t curves by calculations based on Goyal et al.'s experimental data [29] on mercury adsorption on ACC and GAC at three depths H of the fixed beds of these adsorbents (Table 2). Figures 8 and 9 show these curves, and the captions of these figures present the experimental conditions. As these figures demonstrate, the experimental points lie on straight lines with small scatter in all the dynamic adsorption experiments at various adsorbent bed depths, except the case of adsorption on GAC at an adsorbent bed depth of 8 mm, where the dependence is more accurately described by a parabola (Fig. 9, dashed line).

Table 4. Parameters a_0 and a_1 of the approximating straight lines shown in Figs. 5 and 6 and the calculated parameters of their corresponding adsorption processes

Adsorbent	u	a_0	a_1	R^2	k	q_m
ACC	10.167	7.958	0.0366	0.999	0.732	60.084
	7.167	10.196	0.0381	0.989	0.763	52.078
	5	11.998	0.037	0.996	0.74	44.067
GAC	10.167	5.086	0.0298	0.999	0.596	15.264
	7.167	6.682	0.0316	0.997	0.633	13.31
	5	8.00	0.0296	0.996	0.592	11.886

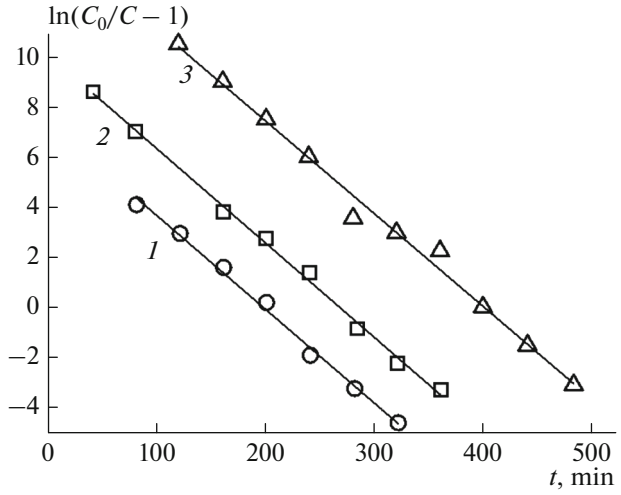

Fig. 8. $\ln(C_0/C-1)$ versus t curves of dynamic adsorption of Hg(II) on the adsorbent ACC at $u = 7.167$ cm/min; $C_0 = 0.05$ mg/mL; and various depths of the fixed adsorbent bed of $H = (1)$ 8, (2) 10, and (3) 15 cm.

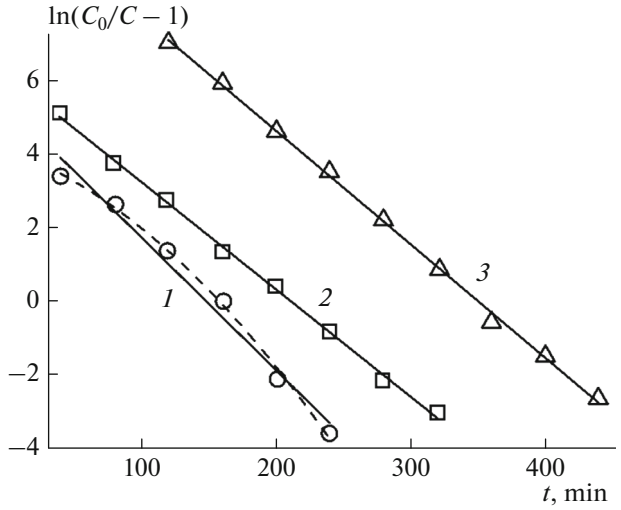

Fig. 9. $\ln(C_0/C-1)$ versus t curves of dynamic adsorption of Hg(II) on the adsorbent GAC at $u = 7.167$ cm/min; $C_0 = 0.05$ mg/mL; and various depths of the fixed adsorbent bed of $H = (1)$ 8, (2) 10, and (3) 15 cm.

The straight lines were obtained by approximating the experimental dependences by Eq. (8). The parabola was calculated during approximation using Eq. (12) at $N = 2$.

The parameters a0 and a1 of the straight lines, determined during the approximation, are presented in Table 5. Table 5 also gives the coefficients of determination $R^2 > 0.99$, which indicate the high quality of approximation of the experimental dependences by straight lines. As already noted, the exception is an attempt to use a straight line to approximate the above dependence of the mercury adsorption on GAC at an adsorbent bed depth of 8 mm. The coefficient of determination in this case is low (0.975), whereas that coefficient in the case of approximation by parabola is 0.994.

Table 5 also presents the adsorption rate constants k and the adsorbent DAC q_m at various fixed-bed depths as calculated by the formulas of Table 1. In the calculations, the adsorbent densities ρ determined in preliminary experiments and given in Table 3 were used. The calculated rate constants k for mercury adsorption on ACC at various fixed-bed depths are similar (0.741–0.755 mL mg^{-1} min^{-1}) and virtually coincide with the values found in the experiments on the adsorption on ACC at various velocities of the liquid being treated of $u = 0.732$–0.763 mL mg^{-1} min^{-1} (Table 4). The mean linear deviation of the constants k determined at various depths of the fixed ACC bed does not exceed 1%.

The straight-line plots of $\ln(C_0/C-1)$ versus t at various H are almost parallel to each other (Fig. 8) because the slopes a_1 of these straight-line plots are similar (0.0371–0.0377). This should be expected because $a_1 = kC_0$ (Table 1), the initial concentrations C_0 in all the experiments are the same (0.05 mg/mL), and the rate constants are independent of the fixed-bed adsorbent depth H.

Table 5 presents the coefficients b_0, b_1, and b_2 of the parabola. Using the values of b_0 and b_1 ($|b_2| \ll |b_0|, |b_1|$), assuming that $a_0 = b_0$ and $a_1 = -b_1$, and applying the formulas of Table 1, we formally calculated the k and q_m values. The latter values differ very significantly from the values obtained at the other depths of the fixed adsorbent bed. We propose a random or severe experimental error as the only explanation of this fact.

Dynamic Adsorption of Nitrate Ions on a Fixed Bed of an Anion-Exchange Resin: Dependence of the Adsorption Process on the Initial Solution Concentration

Yoon et al. [30] studied the adsorption of NO_3^- ions on Cl^--type anion-exchange resin PA408 (Samyang Company Ltd.) in dynamic mode in a continuous column reactor in surface and ground water treatment. Table 6 presents the conditions of Yoon et al. experiments after conversion to units of measure used in this work, where D is the internal diameter of the column, M is the weight of the adsorbent in the column, and C_0 is the initial concentration of NO_3^-.

Because Yoon et al. [30] did not indicate H values, they were calculated using the quantities M, D, and ρ by the formula

$$H = \frac{4M}{\pi D^2 \rho}. \quad (17)$$

The primary data of Yoon et al.'s experiments [30] on dynamic adsorption of nitrate ions on the fixed bed

Table 5. Parameters a_0 and a_1 of the approximating straight lines shown in Figs. 8 and 9 and the calculated parameters of their corresponding adsorption processes

Adsorbent	H	a_0	a_1	R^2	k	q_m
ACC	8	7.407	0.0375	0.994	0.75	48.122
	10	10.098	0.0377	0.997	0.755	52.137
	15	14.833	0.0371	0.991	0.741	51.962
GAC	8	5.326	0.0361	0.975	0.722	11.625
	10	6.14	0.0292	0.998	0.584	13.250
	15	10.773	0.0309	0.999	0.618	14.661
	8*	b_0	b_1	b_2	0.9942	0.267	24.304
		4.114	−0.0133	−8.145E−5			

* Approximation by parabola.

of the anion-exchange resin were represented as breakthrough curves, i.e., dependences of C/C_0 on the volume V of the solution that has passed through the experimental column. For uniformity and convenience of presentation, we converted the breakthrough curves into C_0/C versus t curves.

Similar to what we did above in considering the mercury adsorption on activated carbons, the primary data of Yoon et al. work [30] were also processed according to the BDST model using Eq. (4) or generalized formula (8). Namely, dependences of $\ln(C_0/C-1)$ on t were constructed, and by approximating them by straight lines, parameters given in Table 1 were determined. As already noted, with account of expression (7), the conclusions drawn are also consistent with the Thomas model.

Figure 10 presents the $\ln(C_0/C-1)$ versus t curves we constructed for the dynamic adsorption of nitrate ions on anion-exchange resin PA408 at three different values of the initial solution concentration C_0, which are presented in Table 6. The caption of Fig. 10 gives the experimental conditions. As Fig. 10 shows, the experimental points do not lie on straight lines in all the dynamic adsorption experiments at various initial adsorbate concentrations.

The curves were obtained by approximating the experimental dependences by Eq. (12). It turned out that the fit is satisfactory at $N = 2$, i.e., by parabolas.

Determined during the approximation, the parameters b_0, b_1, and b_2 of the parabolas are given in Table 7. This table also presents the coefficients of determination R^2, which suggest high quality of approximation of the experimental dependences by second-degree polynomials ($R^2 > 0.99$), as well as the adsorption rate constants k and the adsorbent DAC q_m.

The parameters k and q_m were calculated by the formulas

$$k = -b_1/C_0 \tag{18}$$

and

$$q_m = \frac{b_0 u}{kH\rho} \tag{19}$$

with account of the fact that $b_0 = a_0$ and $b_1 = -a_1$ (see Table 1 and expressions (8) and (12)).

Although the experimental dependences were approximated by Eq. (12) at $N = 2$, rather than by Eq. (8), the parameters k and q_m were calculated using expressions (18) and (19), which are analogs of formulas (14) and (16) derived for a linear dependence of $\ln(C_0/C - 1)$ on t. Such an approach is applicable because $|b_2| \ll |b_0|, |b_1|$ (Table 7).

Figure 11 presents the $-b_1$ versus C_0 curve with the equation

$$-b_1 = k/C_0. \tag{20}$$

The values calculated from the experimental data (Table 7) are shown in Fig. 11 by circles. The solid line

Table 6. Experimental conditions

Parameter	Unit of measure	Value
H	cm	2.7
		5.4
D	cm	1.2
M	g	2.0
		4.0
ρ	g/cm^3	0.655
u	cm/min	106.16
		159.24
C_0	mg/mL	0.0072
		0.0145
		0.0218

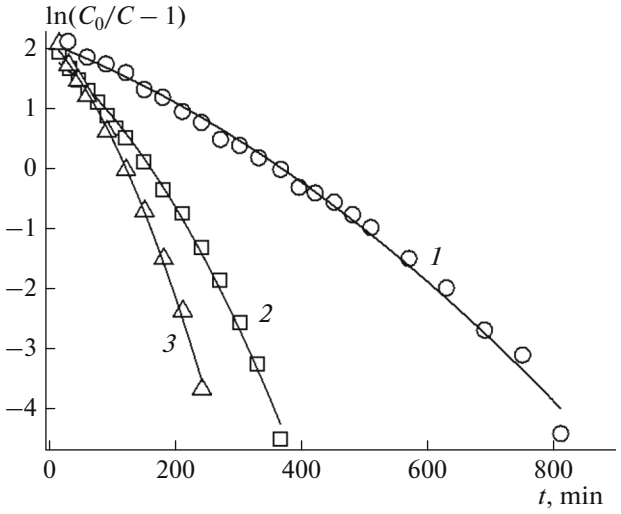

Fig. 10. $\ln(C_0/C-1)$ versus t curves of dynamic adsorption of nitrate ions on the anion-exchange resin PA408 at H = 5.4 cm; u = 159.24 cm/min; and different values of the initial solution concentration C_0 of (*1*) 0.0072, (*2*), 0.0145, and (*3*) 0.0218 mg/mL.

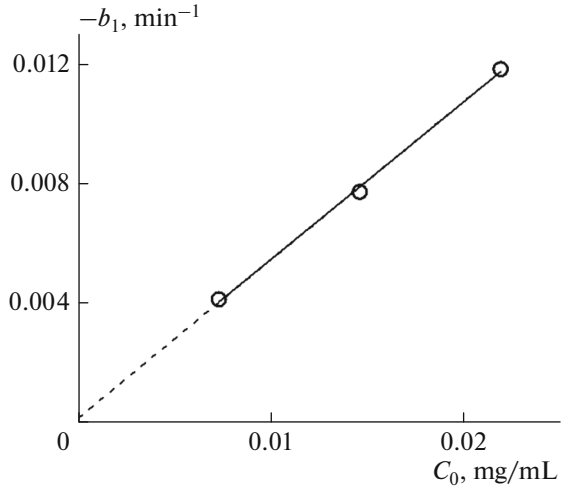

Fig. 11. $-b_1$ versus C_0 curve (see text).

was obtained by approximating the dependence of $-b_1$ on C_0 by relation (20). The dashed line is a continuation of the solid line and is seen to almost pass through the origin of coordinates: the y-intercept calculated during approximation is 2.33×10^{-4}. All this is indicative of the validity of using Eq. (18) for calculating the rate constants k for the adsorption of nitrate ions on Cl^--type anion-exchange resin PA408, although the dependences of $\ln(C_0/C-1)$ on t are not described by straight lines. Note that the k values are virtually independent of C_0: their mean linear deviation at $\bar{k} = 0.548$ is 4%.

The q_m values are within the range 159–179 mg/g (Table 7). Their scatter is seen to be more significant: the mean linear deviation is 6.8%. This can be explained by the fact that the point of intersection of the curves shown in Fig. 10 is not on the y-axis but is shifted to the right along the x-axis.

As a result, the scatter of the b_0 values obtained using y-intercepts is relatively large, and, hence, so is the scatter of values of the capacity q_m, which, according to expression (19), is proportional to b_0. This is due to the fact that, because of the high velocity of the liquid flow being treated (u = 159.24 cm/min), the adsorbate begins to break through immediately after the onset of the dynamic adsorption in the column packed with a freshly prepared adsorbent. This DAC scatter is quite typical for the dynamic adsorption of nitrates. For comparison, the q_m values for adsorption of nitrate ions on a biosorbent [31] are within the range 106–122 mg/g.

The linear dependence of $-b_1$ on C_0 suggests the important conclusion that the adsorbate–adsorbent system under consideration can be described by the BDST (or Thomas) models rather than by the Yoon–Nelson model because, in the latter model, b_1 is independent of C_0.

4. CONCLUSIONS

In summary, we note that the proposed approach to analyzing experimental breakthrough curves of the dependence $C/C_0 = f(t)$ by construction of curves in $\ln(C_0/C-1)$ versus t coordinates with further mathematical processing proved to be fruitful. If breakthrough curves obtained in experiments at various depths of the fixed adsorbent bed, different velocities of the liquid flow being treated, and several initial adsorbate concentrations are analyzed in these coordinates, it would be possible to choose a mathematical model that more adequately describes the adsorbate–adsorbent system under consideration. Approximating

Table 7. Parameters b_0, b_1, and b_2 of the approximating parabolas shown in Fig. 10 and the calculated parameters of their corresponding adsorption processes

C_0	b_0	b_1	b_2	R^2	k	q_m
0.0072	2.0928	−0.00414	-4.172×10^{-6}	0.99259	0.571	164.972
0.0145	1.88483	−0.00773	-2.473×10^{-5}	0.99569	0.532	159.635
0.0218	2.15583	−0.01183	-4.875×10^{-5}	0.99728	0.542	179.141

the plots in the same coordinates by polynomials of a certain degree, one can calculate adsorption rate constants, DAC of adsorbents, and dependences of DAC on the velocity of the liquid flow being treated. Using the proposed approach, we analyzed breakthrough curves taken from literature sources for dynamic adsorption of Hg(II) ions on granulated activated carbon and activated carbon cloth, and dynamic adsorption of NO_3^- on Cl^--type anion-exchange resin PA408. It was found that the dependence of $\ln(C_0/C - 1)$ on t describing the mercury adsorption on activated carbons is linear, whereas such a dependence for the adsorption of nitrate ions on an ion-exchange resin is parabolic. For all these adsorption systems, we calculated adsorption rate constants, DAC of adsorbents, and their dependences on process parameters.

REFERENCES

1. I. V. Kumpanenko, A. V. Roshchin, A. A. Berlin, and B. F. Myasoedov, Khim. Bezopasn. **1** (1), 33 (2017).
2. I. V. Kumpanenko, A. V. Roshchin, N. A. Ivanova, V. V. Novikov, A. M. Skryl'nikov, A. M. Podvalny and V. V. Usin, Russ. J. Phys. Chem. B **11**, 154 (2017).
3. L. A. Jonas and J. A. Rehrmann, Carbon **11**, 59 (1973).
4. A. Wheeler and A. J. Robell, J. Catal. **13**, 299 (1969).
5. L. A. Jonas and W. J. Sevirbely, J. Catal. **24**, 446 (1972).
6. S. H. Lin, C. S. Wang, and C. H. Chang, Ind. Eng. Chem. Res. **41**, 4116 (2002).
7. H. C. Thomas, Ann. N.Y. Acad. Sci. **49**, 161 (1948).
8. Z. Aksu and F. Gonen, Process Biochem. **39**, 599 (2004).
9. M. Ghasemi, A. R. Keshtkar, R. Dabbagh, and S. J. Safdari, J. Hazard. Mater. **189**, 141 (2011).
10. R. Han, D. Ding, Y. Xu, W. Zou, et al., Bioresour. Technol. **99**, 2938 (2008).
11. X. Du, Q. Yuan, and Y. Li, Chem. Eng. Technol. **31**, 1310 (2008).
12. C. Tien, Butterworth-Heinemann Ser. Chem. Eng **11**, 244 (1994).
13. B. Liu, L. Zeng, J. Mao, and Q. Re, Chem. Eng. Technol. **33**, 1146 (2010).
14. G. Grevillot, S. Marsteau, and C. Vallieres, J. Occup. Environ. Hyg. **8**, 279 (2011).
15. F. G. Helfferich and P. W. Carr, J. Chromatogr., A **629**, 97 (1993).
16. G. S. Bohart and E. Q. Adams, J. Am. Chem. Soc. **42**, 523 (1920).
17. V. C. Srivastava, B. Prasad, I. M. Mishra, I. D. Mall, and M. M. Swamy, Ind. Eng. Chem. Res. **47**, 1603 (2008).
18. S. Ayoob, A. K. Gupta, and P. B. Bhakat, Sep. Purif. Technol. **52**, 430 (2007).
19. Z. Xu, J.-G. Cai, and B.-C. Pan, J. Zhejiang Univ. Sci. A: Appl. Phys. Eng. **14**, 155 (2013).
20. R. A. Hutchins, Chem. Eng. Sci. **80**, 133 (1973).
21. J. H. Yoon and J. H. Nelson, Am. Ind. Hyg. Assoc. J. **45**, 509 (1984).
22. S. K. Maji, A. Pal, T. Pal, et al., Sep. Purif. Technol. **56**, 284 (2007).
23. W.-T. Tsai, C.-Y. Chang, C.-Y. Ho, and L. Y. Chen, J. Hazard. Mater. B **69**, 53 (1999).
24. I. V. Kumpanenko, A. V. Roshchin, N. A. Ivanova, A. V. Bloshenko, I. P. Tikhonov, and A. M. Skryl'nikov, Russ. J. Phys. Chem. B **11**, 543 (2017).
25. G. Yan, T. Viraraghavan, and M. Chen, Adsorp. Sci. Technol. **19**, 25 (2001).
26. R. Pearl and L. J. Reed, Proc. Natl. Acad. Sci. U. S. A. **6**, 275 (1920).
27. P. J. Lloyd, Populat. Studies **21**, 99 (1967).
28. R. Pearl and L. J. Reed, Proc. Natl. Acad. Sci. U. S. A. **8**, 365 (1922).
29. M. Goyal, M. Bhagat, and R. Dhawan, J. Hazard. Mater. **171**, 1009 (2009).
30. T. Yoon, Z. H. Shon, G. Lee, et al., Korean. J. Chem. Eng. **18**, 170 (2001).
31. Zhongfei Ren, Xing Xu, Xi Wang, et al., J. Colloid Interface Sci. **468**, 313 (2016).

Translated by V. Glyanchenko